

PAPER

Stylized features of single-nucleon momentum distributions

To cite this article: Jan Ryckebusch *et al* 2015 *J. Phys. G: Nucl. Part. Phys.* **42** 055104

View the [article online](#) for updates and enhancements.

Related content

- [New applications of renormalization group methods in nuclear physics](#)
R J Furnstahl and K Hebeler
- [Coupled-cluster computations of atomic nuclei](#)
G Hagen, T Papenbrock, M Hjorth-Jensen *et al.*
- [Correlations and chargedistributions of medium heavy nuclei](#)
Marta Anguiano and Giampaolo Co'

Recent citations

- [Short range correlations in nuclei and nuclear matter](#)
Arnau Rios
- [Towards understanding astrophysical effects of nuclear symmetry energy](#)
Bao-An Li *et al*
- [Direct Observation of Proton-Neutron Short-Range Correlation Dominance in Heavy Nuclei](#)
M. Duer *et al*

Stylized features of single-nucleon momentum distributions

Jan Ryckebusch, Maarten Vanhalst and Wim Cosyn

Department of Physics and Astronomy, Ghent University, Proeftuinstraat 86, B-9000 Gent, Belgium

E-mail: Jan.Ryckebusch@UGent.be

Received 17 November 2014, revised 21 January 2015

Accepted for publication 9 February 2015

Published 13 March 2015



CrossMark

Abstract

Nuclear short-range correlations (SRC) typically manifest themselves in the tail parts of the single-nucleon momentum distributions. We propose an approximate practical method for computing those SRC contributions to the high-momentum parts. The framework adopted in this work is applicable throughout the nuclear mass table and corrects mean-field models for central, spin–isospin and tensor correlations by shifting the complexity induced by the SRC from the wave functions to the operators. It is argued that the expansion of these modified operators can be truncated to a low order. The proposed model can generate the SRC-related high-momentum tail of the single-nucleon momentum distribution. These are dominated by correlation operators acting on mean-field pairs with vanishing relative radial and angular-momentum quantum numbers. The proposed method explains the dominant role of proton–neutron pairs in generating the SRC and accounts for the magnitude and mass dependence of SRC as probed in inclusive electron scattering. It also provides predictions for the ratio of the amount of correlated proton–proton to proton–neutron pairs which are in line with the observations. In asymmetric nuclei, the correlations make the average kinetic energy for the minority nucleons larger than for the majority nucleons.

Keywords: nuclear reactions, nuclear short-range correlations, electron scattering

(Some figures may appear in colour only in the online journal)

1. Introduction

Momentum distributions contain all the information about the momentum decomposition of the nuclear ground-state wave function. The computation of single-nucleon momentum distributions has reached a very high level of sophistication to date. *Ab initio* methods with variational wave functions can be used to compute the momentum distributions for nuclei up to atomic mass number $A = 12$ [1–5]. Also for atomic mass number infinity, or nuclear matter, advanced many-body calculations with realistic nucleon–nucleon (NN) interactions can be performed [6, 7]. Momentum distributions for mid-heavy and heavy nuclei cannot be computed with *ab initio* methods to date. Advanced approximate schemes like cluster expansions [5, 8, 9] and correlated basis function theory [10, 11] provide momentum distributions for heavier nuclei.

Since the dawn of nuclear physics, the mean-field model has been put forward as a good starting point for understanding the complexity of nuclear dynamics. Important corrections to the mean-field model stem from long-range correlations (LRC) and short range correlations (SRC) [12]. LRC rather affect the low-momentum (infrared) behaviour of the nuclear dynamics, whereas SRC are mostly connected with the high-momentum (ultraviolet) behaviour. As a consequence, by tuning the spatial resolution of the probe used to study nuclei, one can reasonably separate the long-range and short-range phenomena. The focus of this work is on the study of SRC, and LRC are neglected. We wish to put forward a comprehensive theoretical framework to interpret the results of the recent measurements probing SRC, which include studies of the mass and isospin dependence of the SRC. To this end, we present an approximate practical way of computing the SRC contributions to momentum distributions for stable nuclei over the entire mass range.

We start from ground-state wave functions that can be written as correlation operators acting on a single Slater determinant. The computation of expectation values of one-body and two-body operators for those wave functions involves multi-body effective operators and a truncation scheme is in order. We propose a low-order correlation operator approximation, dubbed LCA, that truncates the modified correlated operator corresponding with an one-body operator to the level of two-body operators. The LCA method is specifically designed for dealing with correlations which extend over relatively short distances. For the computation of the single-nucleon momentum distribution, the LCA model developed in section 2, preserves the normalization conditions.

In section 3, we illustrate that the LCA method is a practical approximate way of computing the effect of SRC on single-nucleon momentum distributions for nuclei over the entire mass range. It will be shown that after inclusion of central, spin–isospin and tensor correlations, it can capture some stylized features of nuclear momentum distributions. Due to its wide range of applicability, the LCA framework allows one to study the mass and isospin dependence of SRC and to arrive at a comprehensive picture of the impact of SRC throughout the mass table. We compare the LCA predictions for the high-momentum parts of the single-nucleon momentum distributions for ${}^4\text{He}$, ${}^9\text{Be}$ and ${}^{12}\text{C}$ with those from *ab initio* calculations.

Of course, the LCA approximate method is only justified if the resulting physical quantities like radii and kinetic energies are in reasonable agreement with data and results from more realistic approaches. The impact of SRC on the average nucleon kinetic energies and the root mean square (rms) radii for symmetric and asymmetric nuclei is discussed in section 4. As the correlations induce high-momentum components, they increase the average kinetic energies. The isospin dependence of the SRC is at the origin of some interesting features which depend on the asymmetry of nuclei [7, 13–15]. Also these asymmetry effects will be discussed in section 4.

2. Formalism

A time-honoured method to account for correlations in independent particle models (IPM) is to shift the complexity induced by the correlations from the wave functions to the operators [3, 16]. The correlated ground-state wave function $|\Psi\rangle$ is constructed by applying a many-body correlation operator $\hat{\mathcal{G}}$ to the uncorrelated single Slater determinant $|\Phi\rangle$. The operator $\hat{\mathcal{G}}$ considered in this work, corrects the IPM Slater determinant $|\Phi\rangle$ for SRC:

$$|\Psi\rangle = \frac{1}{\sqrt{\mathcal{N}}} \hat{\mathcal{G}} |\Phi\rangle, \quad (1)$$

with the normalization factor $\mathcal{N} \equiv \langle \Phi | \hat{\mathcal{G}}^\dagger \hat{\mathcal{G}} | \Phi \rangle$. Determining the operator $\hat{\mathcal{G}}$ represents a major challenge [17]. One can be guided, however, by the knowledge of the basic features of the NN force. As far as the short-range nucleon–nucleon (NN) correlations are concerned, $\hat{\mathcal{G}}$ is dominated by the central, spin–isospin and tensor correlations [4, 18, 19]

$$\hat{\mathcal{G}} \approx \hat{\mathcal{S}} \left(\prod_{i < j=1}^A [1 + \hat{l}(i, j)] \right), \quad (2)$$

with $\hat{\mathcal{S}}$ the symmetrization operator and

$$\begin{aligned} \hat{l}(i, j) &= -\hat{g}(i, j) + \hat{s}(i, j) + \hat{t}(i, j) \\ &= -g_c(r_{ij}) + f_{\sigma\tau}(r_{ij}) \vec{\sigma}_i \cdot \vec{\sigma}_j \vec{\tau}_i \cdot \vec{\tau}_j + f_{\tau\tau}(r_{ij}) \hat{S}_{ij} \vec{\tau}_i \cdot \vec{\tau}_j. \end{aligned} \quad (3)$$

Here, \hat{S}_{ij} is the tensor operator and $r_{ij} = |\vec{r}_i - \vec{r}_j|$. Further, $g_c(r_{12})$, $f_{\sigma\tau}(r_{12})$ and $f_{\tau\tau}(r_{12})$ are the central, spin–isospin and tensor correlation functions. The $g_c(r_{12})$ encodes the fact that nucleons have a finite size and forcefully repel each other at short internucleon distances. There is a very strong model dependence in the theoretical predictions for $g_c(r_{12})$ [18, 21]. Predictions range from rather ‘soft’ $g_c(r_{12})$ (with $\lim_{r_{12} \rightarrow 0} g_c(r_{12}) \neq 1$) to ‘hard’ ones (with $\lim_{r_{12} \rightarrow 0} g_c(r_{12}) = 1$) which possess an exclusion zone in the short-distance radial distribution of nucleon pairs. From an analysis of the relative pair momentum distributions in $^{12}\text{C}(e, e'pp)$ experiments [21] one could deduce that the ‘hard’ correlation functions, like the one predicted in the G -matrix calculations by Gearhart [22], provide a fair account of the data. Throughout this work we use the $g_c(r_{12})$ of [22]. The spin–isospin and tensor correlation functions $f_{\sigma\tau}(r_{12})$ and $f_{\tau\tau}(r_{12})$ extend to larger internucleon distances than $g_c(r_{12})$ [20]. We use the $f_{\sigma\tau}(r_{12})$ and $f_{\tau\tau}(r_{12})$ from the variational Monte-Carlo calculations by Pieper *et al* [23]. Note that the $g_c(r_{12})$ of [23] is very soft and severely underestimates the relative-momentum distributions of the $^{12}\text{C}(e, e'pp)$ measurements of [21]. The combination of the three correlation functions considered in this work, has also been used in theory-experiment comparisons for semi-exclusive $A(e, e'p)$ [18, 26] and exclusive $^{16}\text{O}(e, e'pp)$ [24].

Evaluating the expectation value of an operator $\hat{\Omega}$ between correlated states of (1) is far from trivial. The procedure detailed in [16] for example, amounts to rewriting the matrix element between correlated states

$$\langle \Psi | \hat{\Omega} | \Psi \rangle, \quad (4)$$

as a matrix element between uncorrelated states

$$\frac{1}{\mathcal{N}} \langle \Phi | \hat{\Omega}^{\text{eff}} | \Phi \rangle. \quad (5)$$

Hereby, one introduces an effective transition operator $\widehat{\Omega}^{\text{eff}}$ that corrects the operator $\widehat{\Omega}$ for the SRC effects

$$\begin{aligned}\widehat{\Omega}^{\text{eff}} &= \widehat{\mathcal{G}}^\dagger \widehat{\Omega} \widehat{\mathcal{G}} \\ &= \left(\prod_{i < j=1}^A [1 - \hat{l}(i, j)] \right)^\dagger \widehat{\Omega} \left(\prod_{k < l=1}^A [1 - \hat{l}(k, l)] \right).\end{aligned}\quad (6)$$

For the sake of computing single-nucleon momentum distributions, it suffices to consider one-body operators

$$\widehat{\Omega} \equiv \sum_{i=1}^A \widehat{\Omega}^{[1]}(i). \quad (7)$$

In the LCA framework used in this work, a perturbation expansion for (6) is adopted. Thereby, the local dynamical origin of the SRC is exploited to truncate the expansion [16, 25]. Studies of the single-nucleon spectral function in nuclear matter [6] reveal that the correlated part is mainly furnished by three-body breakup processes. For a finite nucleus A this translates into processes with two close-proximity correlated nucleons and a spectator residual $A - 2$ core. This picture has been confirmed in semi-exclusive $A(e, e'p)$ measurements [26, 27]. These observations allow one to treat the SRC as pair correlations to a good approximation. It also justifies a perturbation expansion of (6) that truncates the effective operators $\widehat{\Omega}^{\text{eff}}$ corresponding with a one-body operator $\sum_{i=1}^A \widehat{\Omega}^{[1]}(i)$ to the level of two-body operators. We retain the terms that are linear and quadratic in the correlation operator \hat{l} . The quadratic terms contain terms with both correlation operators acting on the same particle pair. This results in the following effective operator

$$\begin{aligned}\widehat{\Omega}^{\text{eff}} &\approx \widehat{\Omega}^{\text{LCA}} = \sum_{i=1}^A \widehat{\Omega}^{[1]}(i) \\ &\quad + \sum_{i < j=1}^A \left\{ \widehat{\Omega}^{[1],1}(i, j) + \left[\widehat{\Omega}^{[1],1}(i, j) \right]^\dagger + \widehat{\Omega}^{[1],q}(i, j) \right\}.\end{aligned}\quad (8)$$

Here, the linear (l) and quadratic (q) terms read

$$\widehat{\Omega}^{[1],1}(i, j) = \left[\widehat{\Omega}^{[1]}(i) + \widehat{\Omega}^{[1]}(j) \right] \hat{l}(i, j), \quad (9)$$

$$\widehat{\Omega}^{[1],q}(i, j) = \hat{l}^\dagger(i, j) \left[\widehat{\Omega}^{[1]}(i) + \widehat{\Omega}^{[1]}(j) \right] \hat{l}(i, j). \quad (10)$$

The LCA effective operator of (8) has one- and two-body terms, and can be conveniently rewritten as $\widehat{\Omega}^{\text{LCA}} = \sum_{i < j}^A \widehat{\Omega}^{\text{LCA}}(i, j)$ with

$$\widehat{\Omega}^{\text{LCA}}(i, j) = \frac{1}{A-1} \left[\widehat{\Omega}^{[1]}(i) + \widehat{\Omega}^{[1]}(j) \right] + \widehat{\Omega}^{[1],\text{corr}}(i, j), \quad (11)$$

whereby we have introduced a short-hand notation for that part of the operator associated with the correlations

$$\widehat{\Omega}^{[1],\text{corr}}(i, j) = \widehat{\Omega}^{[1],1}(i, j) + \left[\widehat{\Omega}^{[1],1}(i, j) \right]^\dagger + \widehat{\Omega}^{[1],q}(i, j). \quad (12)$$

In the absence of correlations only the first term in the expansion of (8) does not vanish. At medium internucleon distances ($r_{ij} \gtrsim 3$ fm) one has that $\hat{l}(i, j) \rightarrow 0$ and the effective operator

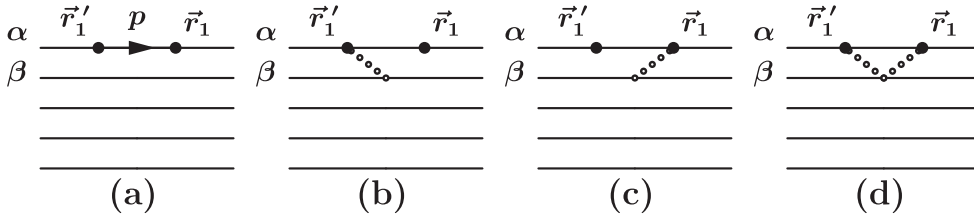


Figure 1. Diagrams (a)–(d) denote the different contributions to the $n^{[1]}(p)$ as it is computed in the LCA. The solid lines denote nucleons in the single-particle state with IPM quantum numbers α, β, \dots and the dotted lines are the correlation operators \hat{l} . Diagram (a) is the IPM contribution to $n^{[1]}(p)$. The other diagrams are the SRC corrections. In the LCA we consider the diagrams that involve two nucleons and are either linear ((b) and (c)) or quadratic (d) in the correlation operators.

$\hat{\Omega}^{\text{LCA}}$ equals the uncorrelated operator $\hat{\Omega}$. The applicability of the LCA method, which involves a truncation of the effective operators to terms which are linear and quadratic in the correlation operators, hinges on the local character of the SRC. LRC, for example, would require an expansion which involves higher-order contributions.

The single-nucleon momentum distribution $n^{[1]}(p)$ quantifies the probability of removing from the nuclear ground state a momentum p at \vec{r}_1' and putting it instantly back at \vec{r}_1 for any combination of (\vec{r}_1, \vec{r}_1') . Accordingly, $n^{[1]}(p)$ is connected to the expectation value of the operator $\hat{\psi}^\dagger(\vec{r}_1)\hat{\psi}(\vec{r}_1')$ (the nucleon field operator $\hat{\psi}(\vec{r}_1')$ annihilates a nucleon at position \vec{r}_1') in the exact ground state Ψ . One can write $\left(d^{3(A-1)}\{\vec{r}_{2-A}\} \equiv \prod_{i=2}^{i=A} d^3\vec{r}_i\right)$

$$n^{[1]}(p) = \int \frac{d^2\Omega_p}{(2\pi)^3} \int d^3\vec{r}_1 d^3\vec{r}_1' d^{3(A-1)}\{\vec{r}_{2-A}\} e^{-i\vec{p}\cdot(\vec{r}_1'-\vec{r}_1)} \Psi^*(\vec{r}_1, \vec{r}_{2-A}) \Psi(\vec{r}_1', \vec{r}_{2-A}). \quad (13)$$

The corresponding single-nucleon operator \hat{n}_p reads

$$\hat{n}_p = \frac{1}{A} \sum_{i=1}^A \int \frac{d^2\Omega_p}{(2\pi)^3} e^{-i\vec{p}\cdot(\vec{r}_i'-\vec{r}_i)} = \sum_{i=1}^A \hat{n}_p^{[1]}(\vec{r}_i, \vec{r}_i') = \sum_{i=1}^A \hat{n}_p^{[1]}(i). \quad (14)$$

The operator \hat{n}_p and the expansion of (11) determine an effective two-body operator \hat{n}_p^{LCA} from which the correlated single-nucleon momentum distributions at momentum p can be computed. The operator \hat{n}_p^{LCA} can be evaluated in the IPM ground-state wave function. The diagrams in figure 1 are a schematic graphical representation of the different contributions to $n^{[1]}(p)$ after introducing the effective operator \hat{n}_p^{LCA} .

In order to preserve the normalization properties $\int dp p^2 n^{[1]}(p) = 1$ in the LCA, the normalization factor \mathcal{N} of (1) is expanded up to the same order as the operator of (11)

$$\mathcal{N} = 1 + \frac{2}{A} \sum_{\alpha < \beta} \text{nas} \langle \alpha\beta | \hat{l}^\dagger(1, 2) + \hat{l}^\dagger(1, 2)\hat{l}(1, 2) + \hat{l}(1, 2) |\alpha\beta \rangle_{\text{nas}}. \quad (15)$$

Here, $|\alpha\beta\rangle_{\text{nas}}$ is the uncoupled normalised and anti-symmetrized (nas) two-nucleon state in the (\vec{r}_1, \vec{r}_2) -space. The summation $\sum_{\alpha < \beta}$ extends over all occupied single-nucleon states. Those states are identified by the quantum numbers $\alpha \equiv n_\alpha l_\alpha j_\alpha m_{j_\alpha} t_\alpha$, whereby t_α denotes the isospin projection.

In order to construct the IPM single-particle wave functions we adopt a harmonic oscillator (HO) basis with a global mass-dependent parametrization

Table 1. The norm \mathcal{N} of (15) for a wide range of nuclei.

^2H	1.128	^{40}Ca	1.637
^4He	1.327	^{48}Ca	1.629
^9Be	1.384	^{56}Fe	1.638
^{12}C	1.435	^{108}Ag	1.704
^{16}O	1.527	^{197}Au	1.745
^{27}Al	1.545	^{208}Pb	1.741

$$\hbar\omega = 45A^{-1/3} - 25A^{-2/3}. \quad (16)$$

In a HO basis, a transformation from (\vec{r}_1, \vec{r}_2) to $(\vec{r}_{12} = \vec{r}_1 - \vec{r}_2, \vec{R}_{12} = \frac{\vec{r}_1 + \vec{r}_2}{2})$ for the nas two-nucleon state can be readily performed [20, 28]

$$|\alpha\beta\rangle_{\text{nas}} = \sum_D |D\rangle \langle D | \alpha\beta \rangle_{\text{nas}}, \quad (17)$$

where we have introduced a shorthand notation for the quantum states of the pairs in the $(\vec{r}_{12}, \vec{R}_{12})$ coordinate space

$$|D\rangle \equiv |nlSjm_j, NLM_L, TM_T\rangle. \quad (18)$$

Here, n and l are the radial and orbital angular-momentum quantum numbers corresponding with the relative motion of the pair. The jm_j are the quantum numbers of the total angular momentum of the pair. The TM_T (S) determine the isospin (spin) quantum numbers of the pair. The c.m. wave function is described by the quantum numbers NLM_L .

Table 1 lists the computed values of the normalization factors of (15) for a range of nuclei from ^2H to ^{208}Pb . The model dependence of the computed \mathcal{N} is related to the choices made with regard to the IPM basis and the correlation functions. Tests for a few nuclei indicate that replacing the HO basis by a Woods–Saxon one changes the computed \mathcal{N} by a few percent. This is connected with the observation that the amount of close-proximity nucleon pairs in a nucleus is rather insensitive to the choice of the single-particle wave functions [20]. The sensitivity of the computed \mathcal{N} to the choices with regard to the correlation functions is larger. For example, after switching off the effect of spin–isospin correlations we find a \mathcal{N} which is about 5% smaller for ^2H and about 10% smaller for the medium-heavy and heavy nuclei listed in table 1.

The deviation of \mathcal{N} from 1 can be interpreted as a quantitative measure for the total effect of the SRC operators on the IPM ground-state wave function. For the deuteron, the tensor correlation operator acting on the relative S -wave of the IPM nucleon pair wave function is responsible for the D -wave component. The LCA is a crude approximation for the proton–neutron deuteron system. Nevertheless, the tail part of the LCA deuteron momentum one-body momentum distribution is in fair agreement with the realistic WCJ1 one [31], which has a 7.3% D -wave admixture. The $a_2(A/{}^2\text{H})$ coefficient is an experimentally determined quantity which is connected with the magnitude of SRC in nucleus A relative to ^2H [32, 33]. It is extracted from the scaling behaviour of the measured $A(e, e')/{}^2\text{H}(e, e')$ cross-section ratio in selected kinematics favouring virtual-photon scattering from correlated pairs. In figure 2, the ratios of the computed norms for A relative to ^2H

$$R_2(A/{}^2\text{H}) = \frac{\mathcal{N}(A) - 1}{\mathcal{N}({}^2\text{H}) - 1}, \quad (19)$$

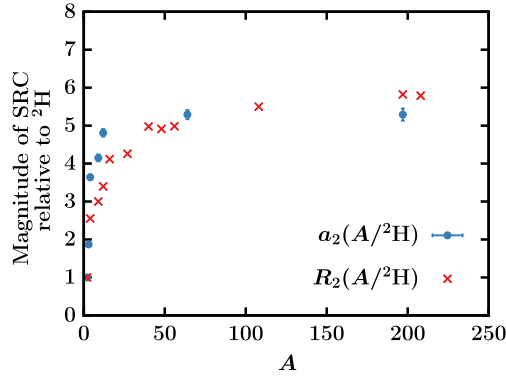


Figure 2. The mass dependence of the computed ratios $R_2(A/{}^2\text{H})$ defined in equation (19) and of the experimentally extracted $a_2(A/{}^2\text{H})$ coefficients from [29].

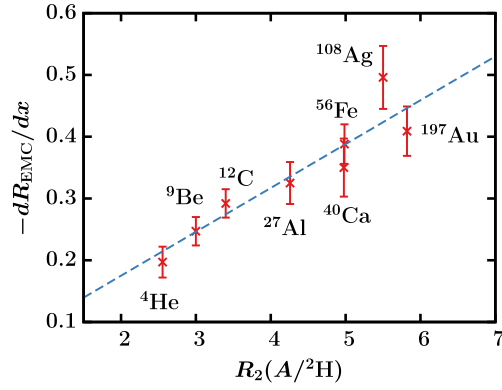


Figure 3. The measured magnitude of the EMC effect, $-\frac{dR_{\text{EMC}}}{dx}$ is plotted as a function of the computed $R_2(A/{}^2\text{H})$ ratios defined in equation (19). The values of the EMC magnitude are from the analysis presented in [30]. The fitted dashed line obeys the equation $-\frac{dR_{\text{EMC}}}{dx} = (0.033 \pm 0.035) + (0.071 \pm 0.009) \cdot R_2(A/{}^2\text{H})$.

are compared to the measured a_2 coefficients of [29]. In the framework developed in this work, the $R_2(A/{}^2\text{H})$ are a measure of the magnitude of the aggregated effect of SRC in nucleus A relative to their magnitude in ${}^2\text{H}$. As can be appreciated from figure 2, the mass dependence of the measured a_2 and computed $R_2(A/{}^2\text{H})$ ratios is roughly the same. For $A \lesssim 40$, $R_2(A/{}^2\text{H})$ increases strongly with mass number A which hints at a strong mass dependence of the quantitative effect of SRC. For $A > 40$, the predicted mass dependence of the magnitude of the SRC is soft.

Recently, it has been suggested that the magnitude of the European muon collaboration (EMC) effect in a specific nucleus A is connected with the magnitude of the SRC in A [34]. Consequently, one can expect a linear relation between the R_2 of equation (19) and the magnitude $-\frac{dR_{\text{EMC}}}{dx}$ of the EMC effect. This suggestion is clearly confirmed in figure 3 which illustrates the correlation between the experimentally extracted $-\frac{dR_{\text{EMC}}}{dx}$ and the LCA

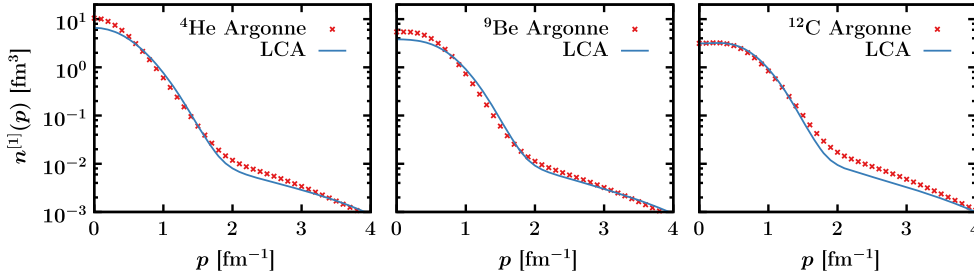


Figure 4. The momentum dependence of the $n^{[1]}(p)$ for ${}^4\text{He}$, ${}^9\text{Be}$ and ${}^{12}\text{C}$. The red crosses are the QMC results of [4] obtained with the Argonne v_{18} two-nucleon and Urbana X three-nucleon potentials.

predictions for the aggregated effect of SRC in nucleus A relative to ${}^2\text{H}$. Clearly, the observed correlation does not imply causation.

3. Single-nucleon momentum distribution

In figure 4 we compare the LCA results for the $n^{[1]}(p)$ with those obtained with quantum Monte-Carlo (QMC) methods using realistic two-nucleon and three-nucleon Hamiltonians [4]. With the normalization factor of (15), the single-nucleon momentum distributions are normalized as $1 = \int dp p^2 n^{[1]}(p)$, which facilitates the comparison over the various nuclei. Up to the characteristic nuclear Fermi momentum $p_F = 1.25 \text{ fm}^{-1}$, the shape of $n^{[1]}(p)$ is very Gaussian in both approaches. For $p > p_F$ the distributions are heavy-tailed. For $p \gtrsim 3 \text{ fm}^{-1}$, the QMC and the LCA method predict a comparable exponential-like fat tail, which is very remarkable given the very different frameworks in which the results are obtained. For medium momenta $p \approx 2 \text{ fm}^{-1}$ the LCA predictions for the $n^{[1]}(p)$ undershoot the QMC ones. This can be attributed to the lack of LRC in the LCA framework. Indeed, the effect of LRC is known to extend to medium nucleon momenta [3, 12]. In the same vein, it is not surprising that for ${}^4\text{He}$ and ${}^9\text{Be}$ the LCA and QMC display some differences at low p , given that LCA does not account for the complicated long-range cluster structures of those nuclei. In this context, it is worth mentioning that the nuclear-matter studies of [7] have clearly illustrated that the fat tails of the single-nucleon distributions are sensitive to the adopted realistic NN interaction. This is related to the fact that the short-range part of the NN force is not well constrained by a fit to NN scattering data.

The LCA results for the $n^{[1]}(p)$ are displayed in figure 5 for a range of nuclei from He to Ag. Some stylized features which apply to all studied nuclei are emerging from the LCA calculations. For $p \lesssim 1.5 \text{ fm}^{-1}$ the distribution is dominated by the IPM contribution (diagram (a) of figure 1) and the SRC do not affect the momentum dependence of $n^{[1]}(p)$. The fat tails are induced by the correlations (diagrams (b), (c) and (d) of figure 1) whereby one distinguishes two regions. For $1.5 \lesssim p \lesssim 3 \text{ fm}^{-1}$ the tensor correlations dominate. The effect of the central correlations extends over a large momentum range and for $p > 3.5 \text{ fm}^{-1}$, it represents the dominant contribution to $n^{[1]}(p)$ (with the tensor part gradually losing in importance). For all nuclei the crossover between the tensor and the central correlated part of the tail of $n^{[1]}(p)$ occurs at a momentum slightly larger than 3 fm^{-1} . At momenta approaching 4 fm^{-1} the central correlations provide about half of the $n^{[1]}(p)$ while the remaining strength is almost exclusively due to the interference between the central and spin-isospin

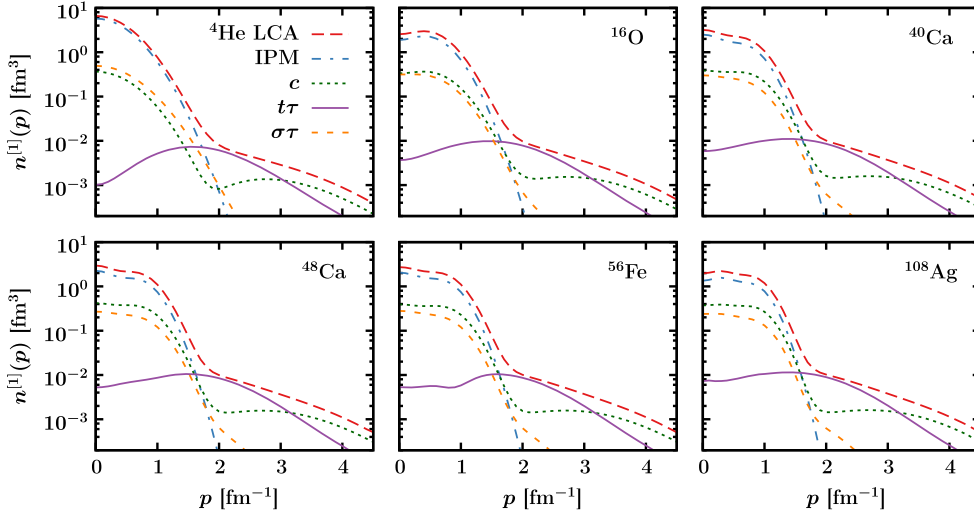


Figure 5. The single-nucleon momentum distribution $n^{[1]}(p)$ for six nuclei. The long dashed line is the full LCA result. The dashed-dotted line is the IPM contribution to the LCA result. Also shown are the results of a calculation that only includes the two-body central (green dotted line), tensor (purple solid line) and spin-isospin (orange short-dashed line) correlation contribution. The LCA result includes the interference between all contributions.

correlations (not shown separately in figure 5). This qualitative behaviour is in line with the *ab initio* ^4He results of [4] (see figure 3 of that reference). The above-mentioned conclusions which apply to the correlated part of the one-body momentum distributions of all nuclei studied here, are qualitatively in line with the nuclear-matter results of [7]. This illustrates that the effect of SRC on single-nucleon momentum distributions can be summarized in some universally applicable principles.

The dominant role of the tensor correlations for intermediate nucleon momenta $1.5 \lesssim p \lesssim 3 \text{ fm}^{-1}$, has some important implications for the isospin dependence of the effect of SRC. With the aid of (11) one can write

$$n^{[1]}(p) = n_{pp}^{[1]}(p) + n_{nn}^{[1]}(p) + n_{pn}^{[1]}(p), \quad (20)$$

with

$$n_{N_1 N_2}^{[1]}(p) = \frac{1}{\mathcal{N}} \sum_{\alpha < \beta} \delta_{t_\alpha, N_1} \delta_{t_\beta, N_2} \text{nas} \langle \alpha \beta | \hat{n}_p^{\text{LCA}}(1, 2) | \alpha \beta \rangle_{\text{nas}}. \quad (21)$$

Referring to figure 1, the $n_{N_1 N_2}^{[1]}(p)$ encodes how much the pp , nn and np pairs contribute to $n^{[1]}$ at given p . The LCA results for $n_{N_1 N_2}^{[1]}(p)$ are shown in figure 6. The ratio $r_{N_1 N_2}(p) \equiv n_{N_1 N_2}^{[1]}(p)/n^{[1]}(p)$ quantifies the relative contribution of $N_1 N_2$ pairs to $n^{[1]}(p)$ at given momentum p . In a naive IPM one expects momentum-independent values of $r_{pp} = \frac{Z(Z-1)}{A(A-1)}$, $r_{nn} = \frac{N(N-1)}{A(A-1)}$ and $r_{pn} = \frac{2NZ}{A(A-1)}$. For $p < p_F$ the plotted ratios in the bottom panel of figure 6 very much follow these naive expectations. The tensor dominated momentum range is characterized by an increase of the pn contribution to $n^{[1]}(p)$.

The above discussion provides a natural explanation for the observation that SRC-sensitive reactions like two-nucleon knockout ($A(e, e'pN)$ and $A(p, ppN)$ reactions for

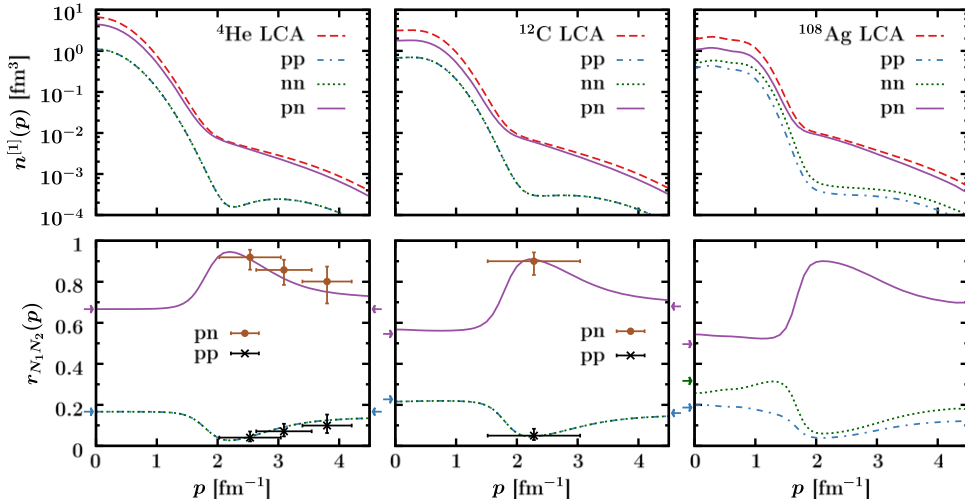


Figure 6. The top panels show the LCA results for the momentum dependence of the contribution of pp pairs ($n_{pp}^{[1]}(p)$), nn pairs ($n_{nn}^{[1]}(p)$), and pn pairs ($n_{pn}^{[1]}(p)$) to the $n^{[1]}(p)$ of ${}^4\text{He}$, ${}^{12}\text{C}$ and ${}^{108}\text{Ag}$. The bottom panels show the momentum dependence of the ratios $r_{N_1N_2} = n_{N_1N_2}^{[1]}(p)/n^{[1]}(p)$ for $N_1N_2 = pp, nn, pn$. The data points for ${}^4\text{He}$ are extracted from the bottom panel of figure 2 in [35]. The data points for ${}^{12}\text{C}$ are extracted from [36]. For ${}^4\text{He}$ and ${}^{12}\text{C}$ the theoretical results for pp overlap almost perfectly with those for nn . The arrows at $p = 0$ indicate the naive IPM predictions for the $r_{N_1N_2}$. The arrows at $p \approx 4.5 \text{ fm}^{-1}$ are the predictions for the $r_{N_1N_2}$ based on the counting of the $nl = 00$ pairs (see text for more details).

example) are very much dominated by the pn channel in the tensor-dominated region which roughly corresponds with $1.5 \lesssim p \lesssim 3 \text{ fm}^{-1}$. The bottom panels of figure 6 suggest that under those conditions the pn channel can represent 90% of the correlated strength, leaving a mere 5% for the pp channel. This prediction seems to be in line with the experimental observations.

Indeed, the small ratio of pp -to- np pairs above the Fermi momentum has been recently established in ${}^{12}\text{C}(e, e'p(p))$, ${}^{27}\text{Al}(e, e'p(p))$, ${}^{56}\text{Fe}(e, e'p(p))$ and ${}^{208}\text{Pb}(e, e'p(p))$, measurements at Jefferson lab [14, 36]. The quoted pp to pn ratio of $\frac{1 \pm 0.3\%}{18 \pm 5\%}$ for ${}^{12}\text{C}$, displayed in figure 6 is compatible with the LCA predictions thereby assuming that the pp and nn contributions are equal for $N = Z$ nuclei. From an analysis of the ratio $\frac{{}^{12}\text{C}(p, ppn)}{{}^{12}\text{C}(p, pp)}$ it could be inferred that the removal of a proton from the nucleus with initial momentum 275–550 MeV c^{-1} is $92^{+8}_{-18}\%$ of the time accompanied by a neutron [37]. Also this result is in line with the LCA predictions for ${}^{12}\text{C}$ contained in figure 6. Our results indicate that similarly large r_{pn}/r_{pp} ratios may be found for heavier nuclei when probing the tensor-dominated tail of the single-nucleon momentum distribution.

Another interesting feature of the results of figure 6 is that the $r_{pp}(p)$ [$r_{pn}(p)$] reaches its minimum (maximum) at $p \approx 2 \text{ fm}^{-1}$. For $p > 2 \text{ fm}^{-1}$ the $r_{pp}(p)$ grows and the $r_{pn}(p)$ decreases. Experimental evidence supporting this prediction has been recently obtained in the simultaneous measurement of exclusive ${}^4\text{He}(e, e'pp)$ and ${}^4\text{He}(e, e'pn)$ at $(e, e'p)$ missing momenta from 2 to 4.3 fm^{-1} [35]. In those measurements, the kinematics is tuned to probe a nucleon at a given momentum $p > p_F$ in conjunction with its correlated partner. These are precisely the SRC induced two-nucleon processes which systematically dominate the LCA

$n^{[1]}(p)$ above the Fermi momentum. One may be tempted to connect $A(e, e'pN)$ cross-sections to two-nucleon momentum distributions (TNMD). First, even after cross-section factorization no direct connection between the cross-sections and TNMD can be established [38]. Second, as has been pointed out in [3] (a nice pictorial description is given in figure 12 of that reference) the correlated part of the TNMD receives large SRC contributions from three-nucleon configurations. Thereby the correlation is mediated through a third nucleon. The exclusive $A(e, e'pN)$ measurements are not kinematically optimized to probe those three-nucleon configurations. The $A(e, e'pN)$ kinematic settings are optimized to probe SRC-related two-nucleon configurations, and it is precisely those configurations which are the source of strength of the tails of the single-nucleon momentum distributions.

The ${}^4\text{He}$ data points shown in figure 6 are extracted from the ${}^4\text{He}(e, e'pp)/{}^4\text{He}(e, e'pn)$ cross-section ratios of [35], whereby we have assumed that $r_{nn} = r_{pp}$. The r_{np} and r_{pp} cannot be directly connected to the ${}^4\text{He}(e, e'pp)/{}^4\text{He}(e, e'p)$ and ${}^4\text{He}(e, e'pn)/{}^4\text{He}(e, e'p)$ cross-section ratios also shown in figure 2 of [35]. Indeed, for $p > p_F$ the $r_{N_1N_2}(p)$ encodes information about correlated pairs, whereas the ${}^4\text{He}(e, e'p)$ cross-sections also contain contributions from other sources like final-state interactions and triple correlations.

For $p > p_F$ the ratio $\frac{r_{pn}(p)}{r_{pn}(p) + r_{pp}(p)}$ can be interpreted as the ratio of the number of SRC proton–neutron pairs to the sum of the proton–neutron and proton–proton ones at a momentum p . In [14] this ratio has been extracted from the combination of $A(e, e'pp)$ and $A(e, e'p)$ measurements for the nuclei ${}^{12}\text{C}$, ${}^{27}\text{Al}$, ${}^{56}\text{Fe}$ and ${}^{208}\text{Pb}$. The experimental values for the ratios are ≈ 0.95 for the four nuclei and are extracted over a bin covering the range $1.5 \leq p \leq 4.5 \text{ fm}^{-1}$. Our calculations, reproduce the observations that for $p > p_F$ the $\frac{r_{pn}(p)}{r_{pn}(p) + r_{pp}(p)}$ are rather mass independent and adopt a value indicative of the dominance of the proton–neutron SRC pairs.

As the central correlations, which are blind for the isospin of the interacting pairs, gain in importance with increasing p one observes in figure 6 that the $r_{N_1N_2}(p)$ ratios gradually approach a limiting value which is different from the IPM values, in particular for heavier nuclei.

The above discussions indicate that the LCA framework in combination with central, tensor and spin–isospin correlations, captures the stylized features of the SRC including its mass and isospin dependence. We now wish to shed light on the underlying physics mechanics of the correlated part of the momentum distribution. More in particular we address the question: ‘What are the quantum numbers of the IPM pairs which are most affected by the correlations?’ This discussion will lead to an understanding of the high p limits in the bottom panels of figure 6.

One can determine the contributions from the relative quantum numbers nl of the IPM pairs to the correlated part of $n^{[1]}(p)$ (denoted by $n^{[1],\text{corr}}(p)$) by means of the expansion of (17). One finds

$$n_{nl,n'l'}^{[1],\text{corr}}(p) = \sum_{\alpha < \beta} \sum_{D,E} \left[\langle D | \alpha\beta \rangle_{\text{nas}} \right]^\dagger \langle E | \alpha\beta \rangle_{\text{nas}} \delta_{nn_D} \delta_{ll_D} \delta_{n'n_E} \delta_{l'l_E} \langle D | \hat{n}_p^{[1],\text{corr}}(1, 2) | E \rangle, \quad (22)$$

where the operator $\hat{n}_p^{[1],\text{corr}}(1, 2)$ and the states $|E\rangle$, $|D\rangle$ have been defined as in (12) and (18). Obviously, one has

$$\sum_{nl} \sum_{n'l'} n_{nl,n'l'}^{[1],\text{corr}}(p) = n^{[1],\text{corr}}(p). \quad (23)$$

The $n_{nl,n'l'}^{[1],\text{corr}}(p)$ that provide the largest contribution to $n^{[1]}(p)$ are shown in figure 7. It is clear that correlation operators acting on $nl = 00$ IPM pairs are responsible for the major fraction of the $n^{[1]}(p)$ for $p \gtrsim 2 \text{ fm}^{-1}$. For heavier nuclei, the contributions from pairs with $n > 0$ and $l = 0$ gain in importance. Non-diagonal $\hat{n}_{nl,n'l'}^{[1],\text{corr}}(p)$ represent a small fraction of the high-momentum tail.

We wish to stress that correlation operators acting on IPM pairs can change the quantum numbers. For example, the tensor operator acting on the deuteron's $l = 0$ IPM pair generates the correlated $l = 2$ state. The dominant role of $nl = 00$ IPM pairs in the creation of high-momentum components, provides support for our proposed method to quantify the SRC by counting the number of $nl = 00$ IPM pairs [20, 28, 38]. Consequently, for high p the central correlations dominate and the $r_{N_1 N_2}(p)$ ratios of figure 6 are connected with the amount of $N_1 N_2$ IPM pairs with $nl = 00$. Using the computed number of $nl = 00$ pairs in ^{12}C we find $r_{pp} = r_{nn} = 0.16$ and $r_{pn} = 0.68$. For ^{108}Ag , a similar calculation leads to $r_{pp} = 0.14$, $r_{nn} = 0.20$ and $r_{pn} = 0.66$. For high p these numbers are fair predictions for the computed ratios $r_{N_1 N_2}(p)$ in figure 6. The dominant role of the $nl = 00$ pairs in generating the high-momentum components of the single-nucleon momentum distributions provides also a natural explanation for the observation that the high-momentum tail of the single-nucleon momentum distributions of nuclei has a universal shape. Indeed, the wave function for the $nl = 00$ pairs does not dramatically change as one moves through the nuclear mass table.

4. Single-nucleon kinetic energies and rms radii

We now turn to a discussion of the LCA predictions for the single-nucleon kinetic energies $\langle T_N \rangle$ and rms radii. The $\langle T_N \rangle$ are not observables but the LCA results can be compared with previously published ones. In addition, in recent publications [39, 40], the isospin dependence of the $\langle T_N \rangle$ has been connected with the kinetic part of the nuclear symmetry energy, which is one of the key bulk properties of atomic nuclei. In a non-relativistic framework, the diagonal single-nucleon kinetic energy operator $\hat{T}^{[1]}$ can be written as

$$\hat{T}^{[1]} = \sum_{i=1}^A \hat{T}^{[1]}(i) = \sum_{i=1}^A \frac{-\hbar^2}{2M_i} \nabla_i^2, \quad (24)$$

where M_i is the nucleon mass. In the IPM, the average kinetic energy $\langle T_p \rangle$ per proton is given by

$$\langle T_p^{\text{IPM}} \rangle = \frac{1}{Z} \sum_{\alpha} \delta_{t_{\alpha}, p} \langle \alpha | \hat{T}^{[1]}(1) | \alpha \rangle. \quad (25)$$

A similar definition is adopted for the average kinetic energy per neutron $\langle T_n \rangle$. In the LCA framework developed in section 2 one has

$$\langle T_p^{\text{LCA}} \rangle = \frac{1}{\mathcal{N}} \frac{1}{Z} \sum_{\alpha < \beta}^{\text{nas}} \langle \alpha \beta | \hat{T}_p^{\text{LCA}}(1, 2) | \alpha \beta \rangle_{\text{nas}}, \quad (26)$$

where the operator \hat{T}_p^{LCA} can be obtained from (11). Since we work in a non-relativistic framework, we have adopted a hard cutoff of 4.5 fm^{-1} for the maximum nucleon momentum in the calculations of the kinetic energy.

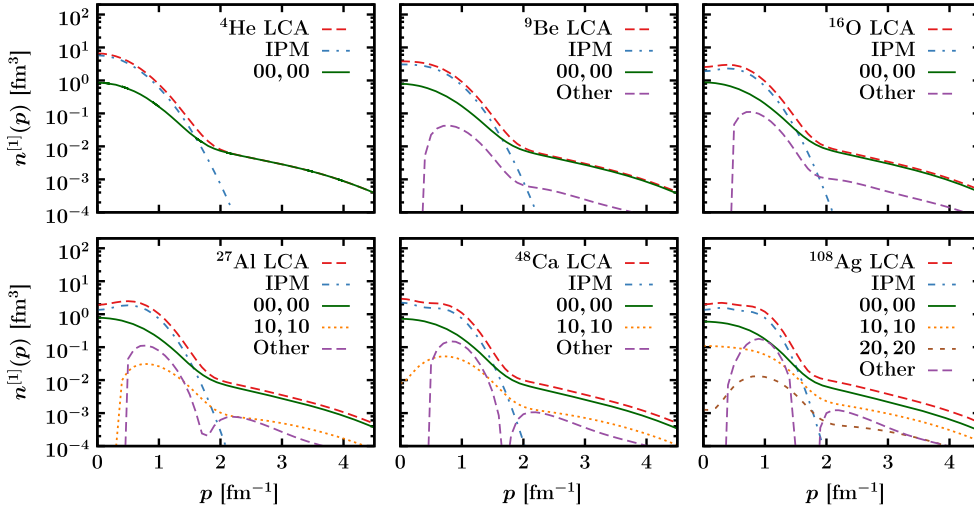


Figure 7. The momentum dependence of the $n^{[1]}(p)$ for six nuclei. The red dashed line is the LCA result. The blue dashed-dotted line is the IPM contribution to the LCA result. Also shown are the $n_{nl,n'l'}^{[1],corr}(p)$ that dominate the high momentum tail. The purple dashed line is the summed contribution of the $n_{nl,n'l'}^{[1],corr}(p)$ which are not shown separately.

Table 2. Results from the IPM and LCA framework for the kinetic energy per proton and neutron ($\langle T_p \rangle$ and $\langle T_n \rangle$) for a variety of nuclei. We compare to values obtained for the average correlated kinetic energy per nucleon $\langle T_N \rangle$ from alternate calculations [43, 44].

A	$x_p = \frac{Z}{A}$	$\langle T_N \rangle$ (MeV)				$\langle T_p \rangle / \langle T_n \rangle$			
		IPM (p)	IPM (n)	LCA (p)	LCA(n)	[43]	[44]	IPM	LCA
^2H	0.500	14.95	14.93	20.95	20.91			1.00	1.00
^4He	0.500	13.80	13.78	25.28	25.23		19.63	1.00	1.00
^9Be	0.444	15.81	16.58	28.91	27.33			0.95	1.06
^{12}C	0.500	16.08	16.06	28.96	28.92	32.4	22.38	1.00	1.00
^{16}O	0.500	15.61	15.59	29.48	29.43	30.9	23.81	1.00	1.00
^{27}Al	0.481	16.61	16.92	30.93	30.26		25.12	0.98	1.02
^{40}Ca	0.500	16.44	16.42	31.23	31.18	33.8	27.72	1.00	1.00
^{48}Ca	0.417	15.64	17.84	33.04	30.06		27.05	0.88	1.10
^{56}Fe	0.464	16.71	17.45	32.33	31.13	32.7		0.96	1.04
^{108}Ag	0.435	16.48	17.81	33.55	31.16			0.93	1.08

Table 2 compares the IPM and LCA predictions for the kinetic energies per proton and neutron. Obviously, as the kinetic energies can be associated with the fourth moments of the $n^{[1]}(p)$, they are highly sensitive to its fat tails. Indeed, inclusion of the correlations increases the $\langle T_p \rangle$ and $\langle T_n \rangle$ by a factor of about two. For the sake of reference, the average kinetic energy of a one-component nuclear Fermi gas is 21 MeV. For the heaviest nuclei studied in this work we find values which are about 50% larger. The LCA results for the average kinetic

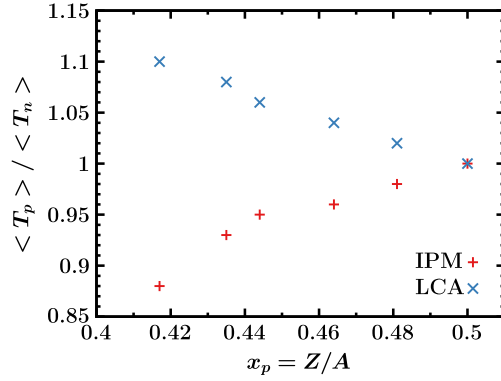


Figure 8. The IPM and LCA predictions for the $\langle T_p \rangle / \langle T_n \rangle$ as a function of the proton fraction x_p .

energies for ${}^9\text{Be}$ are comparable to those of realistic calculations quoted in table 1 of [41]— $\langle T_p \rangle = 29.82$ MeV and $\langle T_n \rangle = 27.09$ MeV. As can be appreciated from table 2, the LCA predictions for the correlated kinetic energies $\langle T_N \rangle$ are comparable with those of the realistic model of [43]. The predictions for $\langle T_N \rangle$ from the variational calculations of [44] are systematically smaller. The ${}^{16}\text{O}$ kinetic energies reported in [23]—obtained using the same spin-isospin and tensor correlation functions as used here—, are about 10% larger than those from the LCA approach (33.7 and 33.8 MeV, compared to 29.4 and 29.5 MeV). Part of this discrepancy can be attributed to the fact that we have imposed a hard momentum cutoff at 4.5 fm^{-1} and this is not present in the calculations of [23]. Incrementing the hard momentum cutoff to 6.0 fm^{-1} , which completely invalidates the use of a non-relativistic framework, increases the LCA predictions for the $\langle T_N \rangle$ with about 15%.

The parameter $x_p = \frac{Z}{A}$ is the proton fraction and is a measure for the asymmetry of nuclei. As expected for a non-interacting two-component Fermi system, $\langle T_p \rangle < \langle T_n \rangle$ for asymmetric nuclei ($x_p < 0.5$) in the IPM. As can be appreciated from figure 8 after inclusion of the correlations, the situation is reversed with the minority component having a larger average kinetic energy. This can be attributed to the tensor correlations, which are stronger between pn than between pp and nn pairs. The difference between $\langle T_p \rangle$ and $\langle T_n \rangle$ increases roughly linearly with decreasing proton fraction x_p . For the most asymmetric nucleus considered here, ${}^{48}\text{Ca}$, $\langle T_p \rangle$ is about 10% larger than $\langle T_n \rangle$.

We now discuss the effect of the correlations on the rms radii of the nuclear matter distribution. The rms radii can be computed with an operator of the form

$$\widehat{r^2} = \frac{1}{A} \sum_i (\vec{r}_i - \vec{R}_{\text{cm}})^2, \quad (27)$$

with $\vec{R}_{\text{cm}} = \frac{1}{A} \sum_i \vec{r}_i$. Using a procedure which is completely similar to the one used for the kinetic energy, in the LCA the operator $\widehat{r^2}$ becomes a correlated operator with a one-body and a two-body part. Table 3 compares the IPM and the LCA predictions for the rms radii. The IPM predictions which are obtained with the global parametrization of (16) tend to overestimate the measured radii for light and heavy nuclei, and underestimate them for mid-heavy nucleus. All in all, the effect of the correlations on the computed rms radii is rather modest. Inclusion of the correlations reduces the rms radii by 8–12%. The reduction factor is

Table 3. Results from the IPM and LCA framework for the rms radii for a variety of nuclei. The results are compared with those from the unitary correlation operator method (UCOM) [44] and experimental values (expt) [42]. All radii are in fm.

A	IPM	LCA	UCOM [44]	Expt [42]
⁴ He	1.84	1.70	1.35	1.6755 ± 0.0028
⁹ Be	2.32	2.13		2.5190 ± 0.0120
¹² C	2.46	2.23	2.36	2.4702 ± 0.0022
¹⁶ O	2.59	2.32	2.28	2.6991 ± 0.0052
²⁷ Al	3.06	2.72	2.82	3.0610 ± 0.0031
⁴⁰ Ca	3.21	2.84	2.93	3.4776 ± 0.0019
⁴⁸ Ca	3.47	3.05	3.20	3.4771 ± 0.0020
⁵⁶ Fe	3.63	3.20		3.7377 ± 0.0016
¹⁰⁸ Ag	4.50	3.94		4.6538 ± 0.0025
¹⁹⁷ Au	5.73	5.21		5.4371 ± 0.0038
²⁰⁸ Pb	5.83	5.28		5.5012 ± 0.0013

hardly dependent on the atomic mass number. Central correlations introduce an exclusion zone around each nucleon and are therefore expected to increase the computed rms radii. The dominant role of the other correlations and the effect of the normalization (which is reflected in the $\frac{1}{N}$ factor in the effective operator) are at the origin of the modest reduction for the rms radii after including the SRC in the LCA framework. The LCA predictions for the rms radii are in acceptable agreement with the experimental values and the predictions from the UCOM framework of [44]. We stress that our IPM results are obtained with a single Slater determinant with HO wave functions from the global parametrization of equation (16). It is likely that one can find a slightly modified parametrization that brings the LCA rms radii closer to the data.

5. Summary

We have introduced an approximate method, dubbed LCA, for the computation of the SRC contributions to the single-nucleon momentum distributions $n^{[1]}(p)$ throughout the whole mass table. A basis of single-particle wave functions and a set of correlation functions serves as an input to LCA. For the numerical calculations presented here, we have included the central, spin–isospin and tensor correlations and mass-independent correlation functions. The LCA method predicts the characteristic high-momentum part of the single-nucleon momentum distribution for a wide range of nuclei. For the light nuclei ⁴He, ⁹Be and ¹²C, the LCA predictions for the tails of the single-nucleon momentum distributions reproduce the stylized features of the QMC ones obtained with realistic Hamiltonians. The predicted aggregated effect of SRC and its mass dependence closely matches the observations from inclusive electron scattering (a_2 coefficients and the magnitude of the EMC effect).

In the LCA, one can separate contributions of the central, spin–isospin and tensor correlations and study how these affect the relative strength of nn , pp and pn pairs in the high-momentum tail of $n^{[1]}(p)$. For $1.5 \lesssim p \lesssim 3 \text{ fm}^{-1}$ the $n^{[1]}(p)$ is dominated by tensor-induced pn correlations. Our prediction for the relative strength of pp and pn pairs in the tail part of $n^{[1]}(p)$ is in line with observations in exclusive two-nucleon knockout studies which point at a strong dominance of np SRC pairs over the pp SRC pairs. We have shown that the high-momentum tail of $n^{[1]}(p)$ is dominated by the correlation operators acting on mean-field pairs

with vanishing relative radial quantum number and vanishing orbital angular momentum, i.e. IPM pairs in a close-proximity configuration. Another prediction of the LCA is that in asymmetric nuclei, the correlations are responsible for the fact that the average kinetic energy of the minority nucleons is larger than for the majority nucleons. The LCA method provides results for the correlated average kinetic energies and nuclear radii which are in line with those of alternate approaches.

Acknowledgments

We thank O Hen and E Piasetzky for many fruitful discussions. This work is supported by the Research Foundation Flanders (FWO-Flanders) and by the Interuniversity Attraction Poles Programme P7/12 initiated by the Belgian Science Policy Office. The computational resources (Stevin Supercomputer Infrastructure) and services used in this work were provided by Ghent University, the Hercules Foundation and the Flemish Government.

References

- [1] Schiavilla R, Wiringa R B, Pieper S C and Carlson J 2007 *Phys. Rev. Lett.* **98** 132501
- [2] Wiringa R B, Schiavilla R, Pieper S C and Carlson J 2008 *Phys. Rev. C* **78** 021001
- [3] Feldmeier H, Horiuchi W, Neff T and Suzuki Y 2011 *Phys. Rev. C* **84** 054003
- [4] Wiringa R B, Schiavilla R, Pieper S C and Carlson J 2014 *Phys. Rev. C* **89** 024305
- [5] Alvioli M, Ciofi degli Atti C, Kaptari L P, Mezzetti C B and Morita H 2013 *Phys. Rev. C* **87** 034603
- [6] Benhar O, Fabrocini A and Fantoni S 1989 *Nucl. Phys. A* **505** 267
- [7] Rios A, Polls A and Dickhoff W H 2014 *Phys. Rev. C* **89** 044303
- [8] Alvioli M, Ciofi degli Atti C and Morita H 2008 *Phys. Rev. Lett.* **100** 162503
- [9] Alvioli M, Ciofi degli Atti C, Kaptari L P, Mezzetti C B, Morita H and Scopetta S 2012 *Phys. Rev. C* **85** 021001
- [10] Ariasde Saavedra F, Bisconti C, Co' G and Fabrocini A 2007 *Phys. Rep.* **450** 1
- [11] Bisconti C, Saavedra F A d and Co' G 2007 *Phys. Rev. C* **75** 054302
- [12] Dickhoff W H and Barbieri C 2004 *Prog. Part. Nucl. Phys.* **52** 377
- [13] Konrad P, Lenske H and Mosel U 2005 *Nucl. Phys. A* **756** 192
- [14] Hen O *et al* 2014 *Science* **346** 614
- [15] Sargsian M M 2014a *Phys. Rev. C* **89** 034305
- [16] Bogner S K and Roscher D 2012 *Phys. Rev. C* **86** 064304
- [17] Neff T and Feldmeier H 2003 *Nucl. Phys. A* **713** 311
- [18] Janssen S, Ryckebusch J, Van Nespen W and Debruyne D 2000 *Nucl. Phys. A* **672** 285
- [19] Ryckebusch J, van der Sluys V, Heyde K, Holvoet H, van Nespen W, Waroquier M and Vanderhaegen M 1997 *Nucl. Phys. A* **624** 581
- [20] Vanhalst M, Ryckebusch J and Cosyn W 2012 *Phys. Rev. C* **86** 044619
- [21] Blomqvist K I *et al* 1998 *Phys. Lett. B* **421** 71
- [22] Gearheart C 1994 *PhD Thesis* Washington University, St. Louis
- [23] Pieper S C, Wiringa R B and Pandharipande V 1992 *Phys. Rev. C* **46** 1741
- [24] Ryckebusch J and van Nespen W 2004 *Eur. Phys. J. A* **20** 435
- [25] Braaten E and Platter L 2008 *Phys. Rev. Lett.* **100** 205301
- [26] Fissum K *et al* (Jefferson Lab Hall A Collaboration) 2004 *Phys. Rev. C* **70** 034606
- [27] Iodice M *et al* 2007 *Phys. Lett. B* **653** 392
- [28] Vanhalst M, Cosyn W and Ryckebusch J 2011 *Phys. Rev. C* **84** 031302
- [29] Hen O, Piasetzky E and Weinstein L B 2012 *Phys. Rev. C* **85** 047301
- [30] Arrington J, Daniel A, Day D B, Fomin N, Gaskell D and Solvignon P 2012 *Phys. Rev. C* **86** 065204
- [31] Gross F and Stadler A 2010 *Phys. Rev. C* **82** 034004
- [32] Fomin N *et al* 2012 *Phys. Rev. Lett.* **108** 092502
- [33] Frankfurt L L, Strikman M I, Day D B and Sargsyan M 1993 *Phys. Rev. C* **48** 2451

- [34] Weinstein L B, Piasetzky E, Higinbotham D W, Gomez J, Hen O and Shneor R 2011 *Phys. Rev. Lett.* **106** 052301
- [35] Korover I *et al* 2014 *Phys. Rev. Lett.* **113** 022501
- [36] Subedi R *et al* 2008 *Science* **320** 1476
- [37] Piasetzky E, Sargsian M, Frankfurt L, Strikman M and Watson J 2006 *Phys. Rev. Lett.* **97** 162504
- [38] Colle C, Cosyn W, Ryckebusch J and Vanhalst M 2014 *Phys. Rev. C* **89** 024603
- [39] Hen O, Li B-A, Guo W-J, Weinstein L B and Piatsetzky E 2015 *Phys. Rev. C* **91** 025803
- [40] Carbone A, Polls A and Rios A 2012 *Europhys. Lett.* **97** 22001
- [41] Sargsian M M 2014b *J. Phys.: Conf. Ser.* **496** 012007
- [42] Angeli I and Marinova K 2013 *At. Data Nucl. Data Tables* **99** 69
- [43] Ciofi degli Atti C and Simula S 1996 *Phys. Rev. C* **96** 1689
- [44] Feldmeier H, Neff T, Roth R and Schnack J 1998 *Nucl. Phys. A* **A632** 61